Picosecond Kinetics of Light Harvesting and Photoprotective Quenching in Wild-Type and Mutant Phycobilisomes Isolated from the Cyanobacterium *Synechocystis* PCC 6803

Lijin Tian,[†] Michal Gwizdala,[‡] Ivo H. M. van Stokkum,[§] Rob B. M. Koehorst,[†¶] Diana Kirilovsky,[‡] and Herbert van Amerongen[†¶*]

[†]Laboratory of Biophysics, Wageningen University, Wageningen, The Netherlands; [‡]Commissariat à l'Energie Atomique, Institut de Biologie et Technologies de Saclay and Centre National de la Recherche Scientifique, Gif sur Yvette, France; [§]Biophysics Group, Department of Physics and Astronomy, Faculty of Sciences, VU University, Amsterdam, The Netherlands; and [¶]MicroSpectroscopy Centre, Wageningen University, Wageningen, The Netherlands

ABSTRACT In high light conditions, cyanobacteria dissipate excess absorbed energy as heat in the light-harvesting phycobilisomes (PBs) to protect the photosynthetic system against photodamage. This process requires the binding of the red active form of the Orange Carotenoid Protein (OCP^r), which can effectively quench the excited state of one of the allophycocyanin bilins. Recently, an in vitro reconstitution system was developed using isolated OCP and isolated PBs from *Synechocystis* PCC 6803. Here we have used spectrally resolved picosecond fluorescence to study wild-type and two mutated PBs. The results demonstrate that the quenching for all types of PBs takes place on an allophycocyanin bilin emitting at 660 nm (APC_Q^{660}) with a molecular quenching rate that is faster than $(1\ ps)^{-1}$. Moreover, it is concluded that both the mechanism and the site of quenching are the same in vitro and in vivo. Thus, utilization of the in vitro system should make it possible in the future to elucidate whether the quenching is caused by charge transfer between APC_Q^{660} and OCP or by excitation energy transfer from APC_Q^{660} to the S_1 state of the carotenoid—a distinction that is very hard, if not impossible, to make in vivo.

INTRODUCTION

The remarkable process of photosynthesis that captures light energy and transforms it into chemical energy is vital for nearly all life on Earth. It is carried out by a wide variety of organisms, such as plants, algae, diatoms, and many species of bacteria. Cyanobacteria, probably being the oldest oxygen-evolving organisms, are believed to have played an essential role in the formation of our planet and our atmosphere ~2.5 billion years ago (1). Even now, they are still active all around the world, living in a large variety of environmental conditions and contributing substantially to the global carbon cycling (2). Like higher plants, they contain photosystems I and II (PSI and PSII) that work in series and are responsible for the splitting of water and the release of oxygen. The central parts of these photosystems, i.e., the reaction centers and the core light-harvesting complexes, are nearly identical for plants and cyanobacteria but the outer light-harvesting complexes are entirely different (3,4): Whereas plants possess intrinsic membrane proteins that all belong to the Lhc family (see, e.g., Croce and van Amerongen (5)), cyanobacteria, like red algae, possess water-soluble phycobilisomes (PBs) that are attached to the PSI- and PSII-containing thylakoid membrane (6).

PBs of *Synechocystis* PCC 6803 (hereafter called *Synechocystis*) are well-organized light-harvesting complexes composed of phycobiliproteins (the phycobilin pigments are open-ring tetrapyrroles) and polypeptides, which are anchored to the stromal side of the thylakoid membrane (6–8). They form a funnel for excitations directed toward PSI and PSII. They comprise approximately six C-phycocyanin (C-PC) rods and three allophycocyanin (APC) core cylinders (Fig. 1). Each C-PC rod is composed of three hexameric disks (18 pigments per hexamer) with a maximum absorbance at 620 nm and maximum fluorescence at 640–650 nm. Each APC cylinder contains four trimer disks (six pigments per trimer), and each trimer has three monomers in which a monomer is a dimer of α^{APC} and β^{APC} polypeptides. Most of the pigments in the APC core have maximum absorbance at 650 nm and maximum emission at 660 nm (APC_{660}) with only a few exceptions: Each of the two APC cylinders closest to the membrane contains two trimers in which one of the α or β APC subunits is replaced by other subunits with bilins of lower excited-state energy (7,9–11).

In one trimer, one polypeptide subunit of α^{APC} in one monomer is replaced by $\alpha^{APC\text{-}B}$ (ApcD) (12) (Fig. 1). And in another trimer, in one monomer both subunits α^{APC}-β^{APC} are replaced; the β^{APC} polypeptide subunit is replaced by $\beta^{APC\text{-}\beta18}$ (ApcF) (12), whereas the α^{APC} polypeptide subunit is replaced by α^{Lcm} (ApcE) (13). ApcE or Lcm is also the core-membrane linker. These modified subunits show maximum fluorescence emission between 676 and 683 nm, and together they are named APC_{680}. These

Submitted January 9, 2012, and accepted for publication March 2, 2012.

*Correspondence: herbert.vanamerongen@wur.nl

Editor: Leonid Brown.

0006-3495/12/04/1692/9 $2.00

doi: 10.1016/j.bpj.2012.03.008

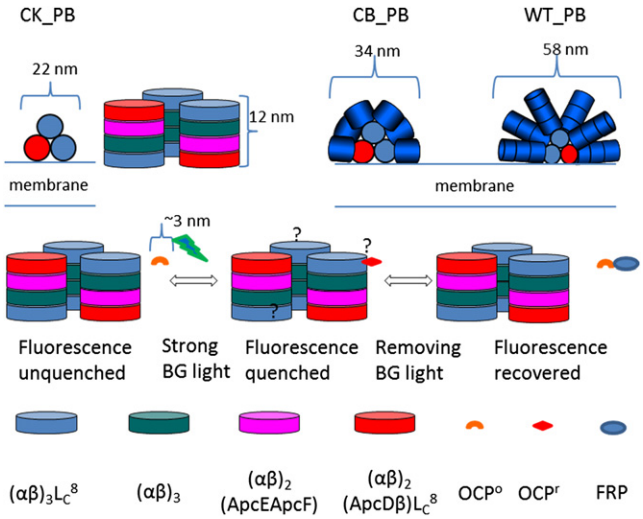

FIGURE 1 Structure of each type of PB is shown schematically. Phycocyanin rods in blue (108 pigments for CB_PB and 324 pigments for WT_PB), allophycocyanin that fluoresces at 660 nm in light blue and bluish green (66 pigments in total), and the low-energy part of allophycocyanin in magenta and red (six pigments in total). The approximate length for each subunit is based on previous work (8,31). The question mark ("?") indicates the potential pigments that OCP^r is interacting with.

low-energy bilins are responsible for direct excitation energy transfer (EET) to the photosystems. Time-resolved fluorescence kinetics of PBs was extensively studied in the past (14–17) and very recently we obtained a comprehensive picture of the entire EET process in wild-type (WT) *Synechocystis* PCC 6803. Various downhill energy-transfer steps within the PBs could be observed, including EET within C_PC with a time constant of 6 ps, EET from C_PC to APC with a time constant of 77 ps, and EET from APC_{660} to APC_{680} with a time constant of 63 ps whereas the uphill back-transfer rates can be calculated using detailed-balance considerations. From APC_{680} excitation, energy is rapidly (exact transfer rates are not known) transferred to the chlorophylls in photosystem I and photosystem II, where charge separation takes place (18).

Cyanobacteria have developed mechanisms that serve to protect the organisms against overexcitation in high-light conditions (19–23). Too-high light intensities cause saturation of the photosynthetic machinery, leading to increased triplet formation on the chlorophylls that in turn causes the production of singlet-oxygen, a highly reactive oxygen species that can lead to severe damage and even the death of the organism (24,25). By increased dissipation of excited-state energy as heat in high-light conditions, a phenomenon called "nonphotochemical quenching" (NPQ), many organisms get rid of excess excitation energy. The underlying molecular mechanisms can strongly vary from species to species and even within the same organism (18,26–29). One of the NPQ mechanisms in cyanobacteria, called the "OCP-related NPQ mechanism", is triggered by strong blue-green light. The OCP-related NPQ mechanism requires the presence of PB and Orange Carotenoid Protein (OCP) in the intact cell (30).

OCP is a water-soluble 35-kDa protein that binds the keto-carotenoid, 3′hydroxyechinenone. The structure of the *Synechocystis* OCP was determined at 1.6 Å (31,32), showing two domains: an α-helical N-terminal domain and an α/β C-terminal domain. OCP is a blue-light-photoactive protein, identified as the trigger of the OCP-dependent NPQ in cyanobacteria. During this OCP-related NPQ mechanism, OCP changes from a stable orange form (OCP^o) into a metastable red form (OCP^r) as a response to strong blue-green light. Unlike OCP^o, the OCP^r form can bind tightly to the APC core, thereby inducing thermal dissipation of the excited PB and concomitantly it quenches the PB fluorescence (33,34). It was reported that in the quenched state, the decrease in excitation energy transfer from the PBs to the photosystems leads to a drop of ~30–40% in the activity of PSI and PSII in *Synechocystis* PCC 6803 cells (35).

In a previous article, we reported on the kinetics of this OCP-dependent nonphotochemical quenching mechanism in vivo and demonstrated that quenching occurs at the level of APC_{660} and the quenching site was termed $APC^Q{}_{660}$. Recently the induction of OCP-related NPQ was successfully reconstructed in vitro using isolated PBs and OCP (33). It was demonstrated that during this process OCP^r is binding to PBs whereas OCP^o is not. Moreover, it was shown that the addition of fluorescence recovery protein can destabilize the binding of OCP^r to PBs and accelerate the fluorescence recovery (33). In that study three different PBs were used: PBs (CK_PBs) from a CK mutant that is completely lacking the C_PC rods (36), PBs (CB_PBs) from a CB mutant that is lacking both the intermediary and the core-distal C_PC hexamers (37), and PBs (WT_PBs) from wild-type cells. The structures of these PBs are shown in Fig. 1. The binding site of OCP^r appeared to be on the allophycocyanin core. It was noticed that the binding of OCP to CK-PBs is weaker than to the other PBs, suggesting an important role of PC rods in the stabilization of the binding.

The fact that this OCP-related NPQ mechanism can now be reconstructed and studied in vitro for PBs with different sizes is important because it provides the possibility to study the physical mechanism underlying the quenching process in vitro making use of ultrafast transient absorption techniques, something that is not easily feasible in vivo. However, this of course requires that the quenching mechanism is the same in vivo and in vitro, and also for the different types of PBs. In this work, we have measured the time- and spectrally resolved fluorescence of three different types of PBs, both in their unquenched and quenched state. The latter state was obtained by complexing the PBs with OCP^r. This should allow us to establish whether the quenching site, rate, and mechanism are the same in vitro and in vivo and to determine what the influence of the PB composition is on the light-harvesting and NPQ properties.

MATERIALS AND METHODS

Isolation of phycobilisomes and formation of OCP-PB complexes

Details about the isolation protocols can be found in the work of Gwizdala et al. (33) and references therein. OCP-PB complexes were prepared in the same way as before at room temperature with an OCP/PB ratio of 40:1 for CK_PB and CB_PB, and with a ratio of 20:1 for WT_PB.

Steady-state fluorescence

Steady-state fluorescence spectra were recorded with a Fluorolog FL3-22 spectrofluorimeter (Horiba Jobin Yvon, Edison, NJ) and corrected for wavelength-dependent sensitivity of the detection and fluctuations in lamp output. The excitation wavelength was 590 nm; a band-pass of either 1 or 2 nm was used for both the excitation and emission monochromator. Fluorescence emission spectra were recorded using a step size of 0.5 nm and an integration time of 0.1 s. OCP-PB complexes were quenched by illuminating WT_PB (for ~5 min) and CB_PB and CK_PB (for ~20 min) at 20°C in 0.8 M phosphate with an actinic white light source in combination with a 500-nm broad band filter (K50) giving an intensity of ~800 $\mu E \cdot m^{-2} \cdot s^{-1}$. Before performing the steady-state fluorescence measurements and inducing nonphotochemical quenching, the optical density of all samples was adjusted to ~0.2 at the absorption maximum for a pathlength of 1 cm. The emission spectra were recorded immediately after quenching. One single measurement was finished in ~30 s, and during this short period, recovery is practically absent for CB_PB and WT_PB, while only a few percent of CK_PB recovers according to Gwizdala et al. (33).

Time-resolved fluorescence

Time-resolved fluorescence spectra were recorded with a (sub-) picosecond streak-camera system combined with a grating (50 grooves/mm, blaze wavelength 600 nm) with the central wavelength set at 700 nm, having a spectral width of 260 nm (for details see (38–40)). Excitation light was vertically polarized, the spot size diameter was typically ~100 μm, and the laser repetition rate was 250 kHz. The detector polarizer was set at magic-angle orientation. An excitation wavelength of 590 nm was used. The sample was stirred with a magnetic stirring bar (rate ~10 Hz) and the laser power at 590 nm was adjusted to 30 $\pm$ 3 μW. Images of 800-ps and 2-ns time window were obtained for WT_PB and for the other samples only the 2-ns time window was used. A high signal/noise ratio was achieved by averaging 100 single images, each obtained after analog integration of 10 exposures of 1.112 s. Images were corrected for background and photocathode shading, and were sliced up into traces of 4-nm width.

The instrument response function (IRF) was described with a double Gaussian shape; in the 2-ns time window, it consists of a Gaussian of ~20-ps full width at half-maximum (FWHM) (90% of IRF area) on top of a Gaussian of 100-ps FWHM (10% of IRF area), whereas in the 800-ps time window, it becomes a Gaussian of ~9-ps FWHM (90% of IRF area) on top of a Gaussian of 60-ps FWHM (10% of IRF area).

For measuring time-resolved fluorescence of PBs in the quenched state, samples of OCP-PBs were first quenched in the same way as was done for the steady-state fluorescence measurements, and then streak images were collected immediately after the induction of the quenching. During one sequence of 100 images, no differences were observed in the lifetimes and spectral shapes for any of the three quenched samples, meaning that the recovery process is sufficiently slow to perform the measurements on quenched samples. Because of the relatively faster recovery from NPQ, OCP-CK_PB data were collected not after but during actinic illumination with blue-green light. The sample volume used for fluorescence excitation/detection was spatially well separated from the actinic light beam (a cylinder of ~5 mm diameter $\times$ 1 cm length) (18); the entire volume of the sample was 4 ml and the sample was stirred continuously. All measurements were performed at room temperature (~20°C) and lasted ~20 min for each sample.

Data analysis

Data obtained with the streak-camera setup were first globally analyzed either with the R package TIMP or its graphical user interface of Glotaran (for details, see the literature (41–43)). The methodologies of global analysis and target analysis are described in van Stokkum et al. (44): with global analysis, the data were fitted as a sum of exponential decays convolved with an IRF and the amplitudes of each decay component as a function of wavelength are called "decay-associated spectra" (DAS). Subsequently, target analysis was performed to obtain the species-associated spectra (SAS), to identify the site of the quenching, and to describe the energy transfer rates between pigment species and to determine the rate of quenching. The kinetic model used here is entirely consistent with the model used for the target analysis of the in vivo data (18).

RESULTS

Fig. 2 shows the fluorescence quenching of PBs in the presence of OCP after strong blue-green light illumination (see Materials and Methods for details). The amount of fluorescence quenching is 84% for CK_PB, 92% for CB_PB, and 89% for WT_PB (percentage of the maximal peak intensity). The results are similar as before (33,45).

To study the energy-transfer processes and the quenching kinetics in different PBs, time-resolved fluorescence measurements were performed with a picosecond streak-camera system (46). An excitation wavelength of 590 nm was used that selectively excites (>90%) APC_{660} in CK_PB or C_PC pigments (>90%) in CB_PB and WT_PB. Streak images of unquenched PBs are shown in Fig. 3, *A*, *C*, *E*, and of OCP-quenched PBs in Fig. 3, *B*, *D*, and *F*. Note that in CK_PB, the spectrum is hardly shifting in time whereas the spectra of the other two types of PBs are clearly shifting to the red, i.e., to longer wavelengths. The shifting is due to EET to pigments that fluoresce at longer wavelengths. A comparison of the left and right panels shows the dramatic shortening of the fluorescence lifetimes for the quenched PBs.

To describe the streak images quantitatively, global analysis was employed, which led to the DAS that are shown in Fig. 4.

The data of unquenched CK_PB can be fitted by two main components as shown in Fig. 4 *A*. The fastest component of 43 ps has a spectrum that has a positive part peaking at 660 nm, and a negative part with similar area peaking at ~680 nm, mainly reflecting EET from APC_{660} to APC_{680}. The 1.6-ns DAS is positive over the entire wavelength region with maximum emission at ~670 nm, mainly reflecting decay of excitations that are thermally equilibrated over APC_{660} and APC_{680}. Global analysis of the data of quenched CK_PB requires at least three lifetime components (see Fig. 4 *B*). The 34-ps DAS exhibits positive amplitude at 660 nm and a negative amplitude at 680 nm. However, in this case the area of the positive part is clearly

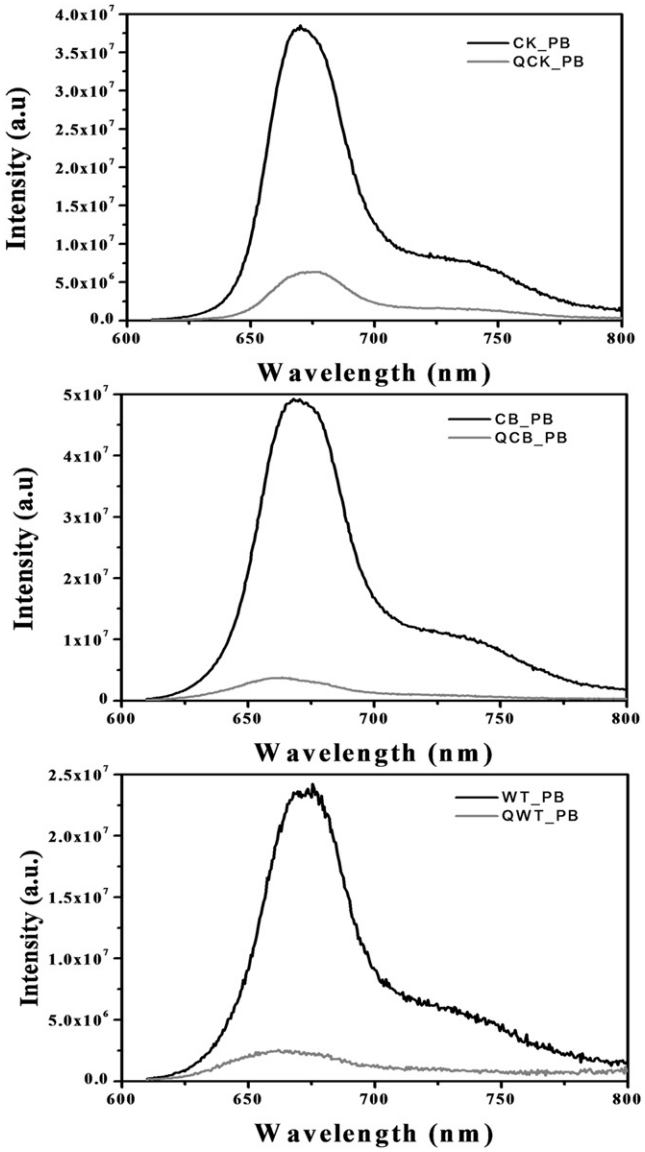

FIGURE 2 Steady-state fluorescence spectra of isolated CK_PBs (*top*), CB_PBs (*middle*), and WT_PBs (*bottom*) before (unquenched, *solid lines*) and after (quenched, *shaded lines*) illumination with high-intensity blue-green light. The fluorescence excitation wavelength is 590 nm. Spectra have been normalized to equal absorption at 590 nm for the unquenched and the quenched PBs.

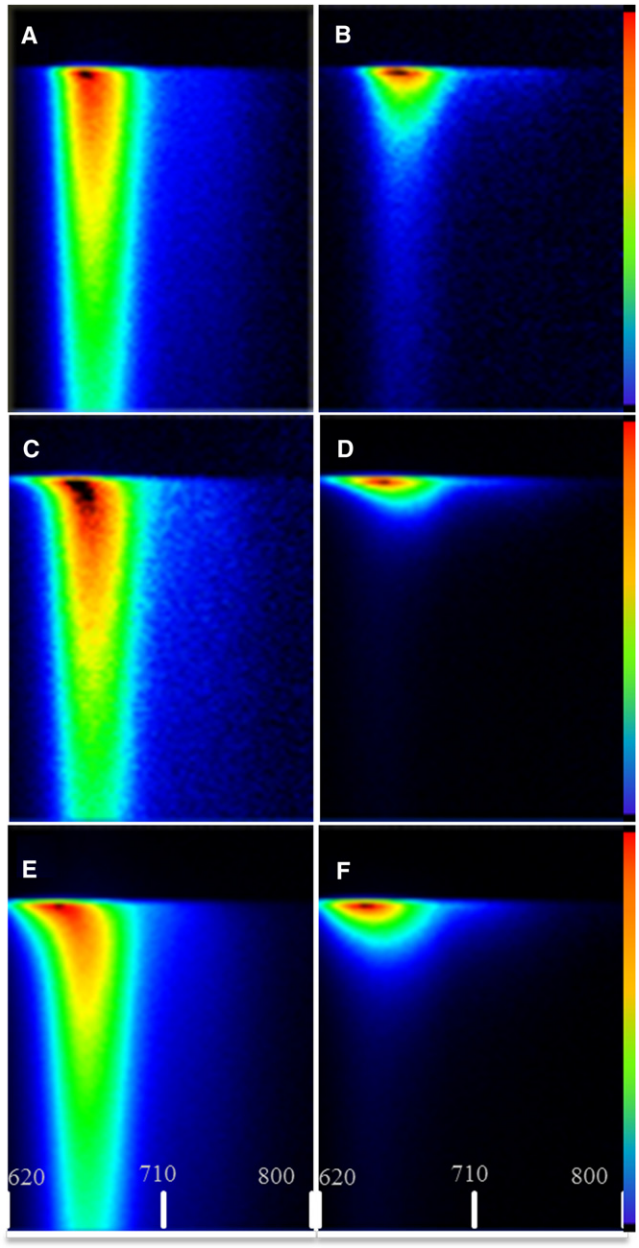

FIGURE 3 Time-resolved fluorescence data obtained with the streak-camera setup using a time window of 2 ns with 590-nm excitation (*A* and *B*) CK_PB, (*C* and *D*) CB_PB, and (*E* and *F*) WT_PB. (*A*, *C*, and *E* correspond to unquenched PBs and *B*, *D*, and *F* correspond to quenched PBs.) All images represent the fluorescence intensity (using a linear color gradient) as a function of time (*vertical axis*, 2 ns) and wavelength (*horizontal axis*, nm).

larger than that of the negative part, and also larger than the positive part of the 43 ps-DAS for unquenched CK_PB. This suggests that substantial excited-state decay already occurs on a timescale of tens of ps, leading to accelerated depopulation of excited APC_{660} molecules and concomitantly a decreased amount of EET to APC_{680}. It should be noted that the negative part of the DAS is not completely disappearing, which is partly due to the fact that not all PBs are quenched (see below). The 197-ps component corresponds to quenched PBs, whereas the 1338-ps component corresponds to some unquenched species, which has a somewhat blue-shifted DAS as compared to the 1.6-ns DAS in unquenched CK_PB. This is probably due to the presence of a small amount of not-well-connected PBs or disconnected APC_{660} trimers.

Fig. 4, *C* and *D*, shows the global-analysis results of unquenched and quenched CB_PB, with three and four components, respectively. For CB_PB, the obtained 19-ps DAS has more or less a conservative spectral shape with a

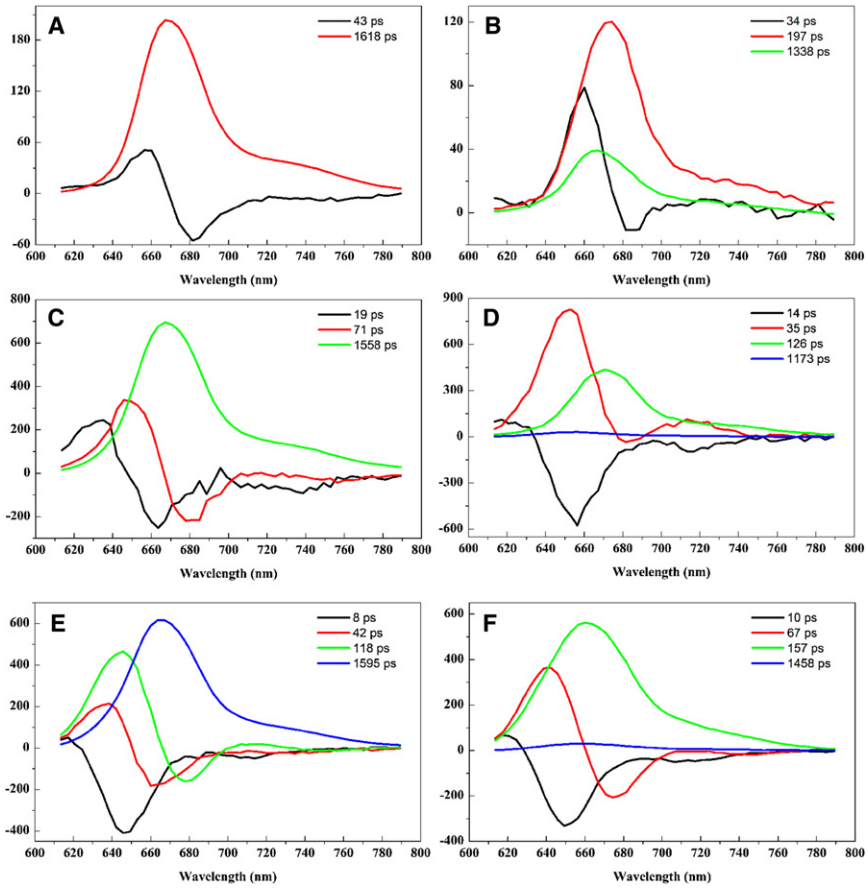

FIGURE 4 Global-fitting results (*DAS*) of the time-resolved fluorescence data obtained with the streak-camera setup using either a time window of 2 ns or 800 ps. (*A* and *B*) CK_PB and OCP-CK_PB after strong blue-green light illumination; (*C* and *D*) CB_PB and OCP-CB_PB after strong blue-green light illumination; (*E* and *F*) WT_PB and OCP-WT_PB after strong blue-green light illumination. The corresponding lifetimes are presented in each figure. Spectra have been normalized to an equal number of absorbed photons at 590 nm, both for the unquenched and the quenched PBs.

positive peak at 635 nm and a negative one at 660 nm, which represents, to a large extent, EET from C_PC to APC_{660}. The 71-ps component is positive at 650 nm and negative at 677 nm, reflecting EET to APC_{680}. An all-positive spectrum of 1.6 ns is peaking at 670 nm. Blue-green-light quenching causes dramatic changes in the DAS, as is shown in Fig. 4 *D*: the fastest component (14 ps) of the quenched state has a dominating negative peak at ~660 nm, with higher amplitude than the 19-ps component of the unquenched state. In contrast, the second component (35 ps) has a larger positive amplitude than the second component (71 ps) for the unquenched complex, also peaking at ~650 nm. The lifetime is much shorter and the negative part peaking at ~680 nm is strongly reduced. The all-positive DAS with a lifetime of 126 ps has a spectral shape that is similar to that of the 1.6-ns component of the unquenched PBs that corresponds to the disappearance of equilibrated excited-state energy, mainly due to quenching. In addition, the spectral shape and lifetime are also similar to those of the 197-ps component of the CK_PB. The longest lifetime component of 1.2 ns peaking at ~650 nm has a small amplitude (~3%) and probably relates to a small amount of free PC species.

Both for the unquenched and quenched WT_PBs, four components are needed to get satisfactory fits of the data. Three clear EET steps can be observed (Fig. 4 *E*). The DAS of the fastest component of 8 ps is almost entirely negative with a peak at ~645 nm. This reflects EET within C-PC from blue pigments with relatively low dipole strength to somewhat more red-shifted pigments with higher dipole strength (18). The 42-ps component shows a positive peak at 640 nm and a negative one at 663 nm and mainly reflects EET from C-PC to APC_{660} (see also Tian et al. (18)). The 118-ps component has a positive peak at ~645 nm and a negative one at 680 nm, reflecting EET to APC_{680}. The 1.6-ns DAS has its main peak at 667 nm, which is due to decay of excited-state-equilibrated PBs.

Under quenching conditions, the fastest component is hardly influenced, indicating that the quenching is not happening on the pigments in C_PC. The 67-ps DAS has a typical EET shape and it is more or less the average of the 42-ps and 118-ps components that are observed for the unquenched PBs. The long-lived DAS (1595 ps) that was observed for the unquenched PBs is now absent, and instead, a similar DAS is observed with a far shorter lifetime of 157 ps. Finally, a small contribution is observed characterized by a lifetime of 1.5 ns and a blue-shifted (as compared to the 157-ps component) emission spectrum, possibly originating from a small fraction of unconnected C_PC.

DISCUSSION

As was shown above, the binding of the activated form of OCP to the different types of PBs in vitro leads to strong changes in the steady-state and time-resolved fluorescence properties of the PBs. It was demonstrated before that for WT *Synechocystis* cells in vivo, OCP-induced NPQ leads to the direct quenching of APC_{660} with a quenching rate of $(\sim 15\ ps)^{-1}$ (18). The fact that OCP is able to induce fluorescence quenching in PBs lacking one or two of the APC_{680} indeed confirmed that the site of quenching must be APC_{660} (11). It is important to note that, in WT *Synechocystis* cells, only 30% of the PBs was quenched due to the presence of substoichiometric amounts of OCP with respect to the amount of PBs, which was probably caused by the fact that the cells were grown in relatively low-light conditions. In OCP overexpressing strains, within a PSI/PSII, less *Synechocystis* mutant, and in strains growing in high-light conditions, high quantities of OCP are present in the cell and concomitantly a high percentage of fluorescence quenching is observed (34,45,47). To sort out whether, in vitro, APC_{660} is also the quencher in complexes of PBs with activated OCP, and to determine the fraction of quenched PBs and the rate of quenching, we have performed target analysis.

Different compartmental models were constructed (see Fig. 5) in analogy with our recent study on entire cells to fit/describe the data (18). Each compartment is composed of a pool of pigments with similar fluorescence spectra. The fitting results for the isolated PBs are also shown in Fig. 5. For all compartments, SAS and also the rates of excitation-energy transfer between different compartments were estimated. All spectra and most of the transfer rates are nearly identical to those obtained for intact cells. The quenching site and rate for each PB were estimated by fitting both unquenched and quenched datasets simultaneously; more details about the fittings are given in the Supporting Material.

The target analysis for CK_PB is relatively simple because only two compartments are needed as shown in Fig. 5; one corresponds to APC_{660} and the other to APC_{680}, and the corresponding spectra are given in blue and red, respectively. One more C_PC spectrum (in *blue*) could be resolved for CB_PB, corresponding to C_PC. For WT_PB two C_PC pools could be resolved (shown as *blue*) and the model established here for WT_PBs is identical to the one obtained for whole cells in vivo (18). Note that there are always some free species with green SAS as shown in Fig. 5 present in CB or WT with a contribution of 5~6%, decaying with a lifetime at ~1 ns.

It is found that quenching only happens on 85% of the CK_PBs under our experimental conditions, whereas 100% of the CB_PBs and WT_PBs appear to be quenched.

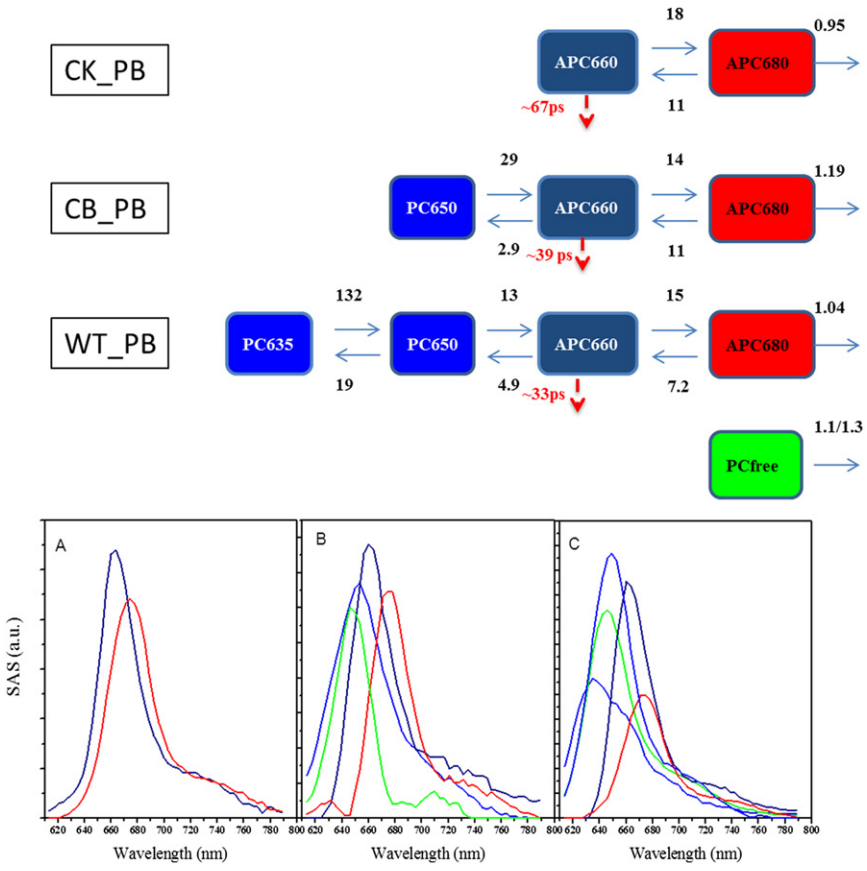

FIGURE 5 Kinetic schemes for target analysis of the time-resolved fluorescence data of unquenched and quenched isolated PBs. Each compartment represents a pool of pigments. Energy-transfer rates between these pools (shown in ns^{-1}) and their spectra were estimated from the fitting: (*A*) CK_PB, (*B*) CB_PB, and (*C*) WT_PB. (*Red*) Inverse quenching rate (in picoseconds). Note that according to the fitting results not all CK_PBs contain a quencher; details are given in the text.

The compartment in which the quenching takes place is unequivocally the one of APC_{660} in all cases. The quality of the fitting decreases substantially and/or unrealistic SAS values are obtained when it is assumed that quenching occurs in one of the other compartments (for further details, see the Supporting Material). If we fit the data to the kinetic scheme of WT_PB in Fig. 5 and we require the quencher to be in compartment 3, then the estimated SAS peaks at ~660 nm. If the quencher is forced to be in compartment 4, the fitting at early times becomes worse (compare to Fig. S2 in the Supporting Material) but the peak of the SAS of the quenched compartment is again ~660 nm. It is inherent to the (early) kinetic data that the quenching takes place in the APC_{660} compartment, no matter what the exact details of the kinetic scheme are. Therefore, the location of the quenching appears to be the same as in vivo (18). The quenching rate for CK_PB is $(67 \pm 7 \text{ ps})^{-1}$ whereas it is $(39 \pm 4 \text{ ps})^{-1}$ for CB_PB and $(33 \pm 3 \text{ ps})^{-1}$ for WT_PB.

It was observed before that the relative amount of quenching for isolated PBs increases in the following order: CK_PB, WT_PB, and CB_PB (33). These results were reproduced in this study (Fig. 2). The target analysis results enable us to estimate the contribution of each compartment to the total steady-state spectrum both for the quenched and unquenched PBs and to determine the origin of the changing quenching ratios. The reconstructed spectra and the corresponding quenching ratios are shown in Fig. S6, Fig. S7, and Fig. S8 and are fully in agreement with the previously observed results (33).

Concerning the quenching mechanism, the quenching rates of $(39 \pm 4 \text{ ps})^{-1}$ in CB_PB and $(33 \pm 3 \text{ ps})^{-1}$ in WT_PB are (only) somewhat slower than the one of $(16 \pm 4 \text{ ps})^{-1}$ obtained for intact cells. It was concluded before that the rate of $(16 \pm 4 \text{ ps})^{-1}$, which corresponds to a quenching rate of the excited state of the pigment that is directly quenched (APC^{Q}_{660}), is extremely fast (18)—namely $(240 \pm 60 \text{ fs})^{-1}$ $(= (16 \pm 4 \text{ ps})^{-1}/66$, where 66 is the number of APC_{660} pigments) or even faster. In our case, the molecular quenching rate must also be extremely fast, namely $(500 \pm 50 \text{ fs})^{-1}$ or faster. Both the similar fast quenching rate and the same identity of the quenched species leave little doubt that the quenching in vitro proceeds via the same mechanism as in vivo. It was suggested in our previous work that quenching is most likely caused by charge transfer between APC^{Q}_{660} and the OCP carotenoid hECN in its activated form but it could not be entirely excluded that EET from APC^{Q}_{660} to the S1 state of hECN might be responsible for this OCP-related NPQ mechanism (18).

Both processes depend critically on the mutual interactions (overlap of molecular wavefunctions) and slight structural differences in the complex between OCP and APC^{Q}_{660} are probably responsible for the differences in quenching rate. Ultrafast transient absorption measurements will be needed to discriminate between these two possibilities. Whereas these measurements are extremely demanding if not impossible for intact cells, they can now be performed on quenched PBs in vitro, because apparently the quenching mechanism is the same. It is of relevance to mention that although the in vitro quenching rate is still extremely fast it would only lead to quenching of ~66% of the excitations in the PBs in vivo whereas the previously determined percentage is 80% in vivo. This percentage of 66% can be calculated using the fact that the rate of transfer from APC to the photosystems is $(63 \text{ ps})^{-1}$ and the rate of quenching is directly competing with this transfer rate (18). Therefore, the extremely fast quenching rate that is obtained in vivo is crucial for the efficiency of quenching.

It is of interest to note that the quenching in CK_PB is even slower $(67 \text{ ps})^{-1}$, which suggests that the presence of C_PC is required for the tight binding between OCP^{r} and PBs. It was already reported before that the binding of OCP to CK_PB is weaker than to WT_PB and CB_PB (33), and now it is found that this leads not only to a lower percentage of quenched PBs but also to a slower quenching rate. With this rate of quenching, the efficiency of quenching would be ~50% in vivo. The slower quenching rate and the lower binding strength both contribute to explain the low amplitude of fluorescence quenching observed in CK cells compared to that observed in WT cells (30).

CONCLUSIONS

All types of isolated PBs that were studied here show a large amount of nonphotochemical quenching upon binding of the red active form OCP. In all cases, the quenching occurs in the core of the PBs on APC_{660} and not on APC_{680}. However, also the presence of C_PC has some influence on the quenching, because the rate of quenching increases from $(67 \pm 7 \text{ ps})^{-1}$ for CK_PB to $(39 \pm 4 \text{ ps})^{-1}$ for CB_PB and $(33 \pm 3 \text{ ps})^{-1}$ for WT_PB. Although the latter rate is still a factor-of-2 slower than the one in vivo, it is concluded that both the site and mechanism of quenching are the same in all PBs, both in vitro and in vivo. Full assembly in vivo leads to the fastest quenching rate, and this rate is required to compete with excitation-energy transfer to the photosystems, allowing efficient photoprotection.

SUPPORTING MATERIAL

Eight figures are available at http://www.biophysj.org/biophysj/supplemental/S0006-3495(12)00290-1.

We thank Arie van Hoek (Wageningen University and Research Center) for excellent technical support.

This work was supported by a fellowship to L.T. by the Graduate School Experimental Plant Sciences, Wageningen, The Netherlands, and by the European community via the HARVEST project and by the Dutch Ministry of ELI through the BioSolar Cells Project. M.G. is supported by the European community via a fellowship of the HARVEST project. Research in D.K.'s group is supported by the Commissariat à l'Energie Atomique,

Centre National de la Recherche Scientifique, and (l'Agence Nationale de la Recherche (CYANOPROTECT), France.

REFERENCES

1. Rasmussen, B., I. R. Fletcher, …, M. R. Kilburn. 2008. Reassessing the first appearance of eukaryotes and cyanobacteria. *Nature.* 455:1101–1104.
2. Potts, B. A. W. M. 2002. The Ecology of Cyanobacteria: their Diversity in Time and Space. Kluwer Academic Publishers, Dordrecht, The Netherlands.
3. Golbeck, J. H. 1992. Structure and function of Photosystem-I. *Annu. Rev. Plant Physiol.* 43:293–324.
4. Barber, J., and J. Nield. 2002. Organization of transmembrane helices in photosystem II: comparison of plants and cyanobacteria. *Philos. Trans. R. Soc. Lond. B Biol. Sci.* 357:1329–1335, Discussion 1335, 1367.
5. Croce, R., and H. van Amerongen. 2011. Light-harvesting and structural organization of Photosystem II: from individual complexes to thylakoid membrane. *J. Photochem. Photobiol. B.* 104:142–153.
6. Adir, N. 2005. Elucidation of the molecular structures of components of the phycobilisome: reconstructing a giant. *Photosynth. Res.* 85:15–32.
7. Glazer, A. N. 1984. Phycobilisome—a macromolecular complex optimized for light energy-transfer. *Biochim. Biophys. Acta.* 768:29–51.
8. Arteni, A. A., G. Ajlani, and E. J. Boekema. 2009. Structural organization of phycobilisomes from *Synechocystis* sp. strain PCC6803 and their interaction with the membrane. *Biochim. Biophys. Acta.* 1787:272–279.
9. Lundell, D. J., and A. N. Glazer. 1983. Molecular architecture of a light-harvesting antenna. Core substructure in *Synechococcus* 6301 phycobilisomes: two new allophycocyanin and allophycocyanin B complexes. *J. Biol. Chem.* 258:902–908.
10. Sidler, W. 1994. Phycobilisome and phycobilisome structure. *In* The Molecular Biology of Cyanobacteria. D. A. Bryant, editor. Kluwer Academic Publishers, Dordrecht, The Netherlands. 139–261.
11. Jallet, D., M. Gwizdala, and D. Kirilovsky. 2011. ApcD, ApcF, and ApcE are not required for the orange carotenoid protein-related phycobilisome fluorescence quenching in the cyanobacterium *Synechocystis* PCC 6803. *Biochim. Biophys. Acta*. http://www.sciencedirect.com/science/article/pii/S0005272811002921.
12. Lundell, D. J., and A. N. Glazer. 1983. Molecular architecture of a light-harvesting antenna. Structure of the 18 S core-rod subassembly of the *Synechococcus* 6301 phycobilisome. *J. Biol. Chem.* 258:894–901.
13. Redlinger, T., and E. Gantt. 1982. A M^r 95,000 polypeptide in *Porphyridium cruentum* phycobilisomes and thylakoids: possible function in linkage of phycobilisomes to thylakoids and in energy transfer. *Proc. Natl. Acad. Sci. USA.* 79:5542–5546.
14. Suter, G. W., P. Mazzola, …, A. R. Holzwarth. 1984. Fluorescence decay kinetics in phycobilisomes isolated from the bluegreen alga *Synechococcus* 6301. *Biochim. Biophys. Acta.* 766:269–276.
15. Mullineaux, C. W., and A. R. Holzwarth. 1991. Kinetics of excitation-energy transfer in the cyanobacterial phycobilisome-Photosystem-II complex. *Biochim. Biophys. Acta.* 1098:68–78.
16. Bittersmann, E., and W. Vermaas. 1991. Fluorescence lifetime studies of cyanobacterial Photosystem-II mutants. *Biochim. Biophys. Acta.* 1098:105–116.
17. Krumova, S. B., S. P. Laptenok, …, H. van Amerongen. 2010. Monitoring photosynthesis in individual cells of *Synechocystis* sp. PCC 6803 on a picosecond timescale. *Biophys. J.* 99:2006–2015.
18. Tian, L., I. H. van Stokkum, …, H. van Amerongen. 2011. Site, rate, and mechanism of photoprotective quenching in cyanobacteria. *J. Am. Chem. Soc.* 133:18304–18311.
19. Kirilovsky, D. 2007. Photoprotection in cyanobacteria: the orange carotenoid protein (OCP)-related non-photochemical-quenching mechanism. *Photosynth. Res.* 93:7–16.
20. Karapetyan, N. V. 2007. Non-photochemical quenching of fluorescence in cyanobacteria. *Biochemistry (Mosc.).* 72:1127–1135.
21. Ihalainen, J. A., S. D'Haene, …, J. P. Dekker. 2005. Aggregates of the chlorophyll-binding protein IsiA (CP43′) dissipate energy in cyanobacteria. *Biochemistry-Us.* 44:10846–10853.
22. Yeremenko, N., R. Kouril, …, J. P. Dekker. 2004. Supramolecular organization and dual function of the IsiA chlorophyll-binding protein in cyanobacteria. *Biochemistry.* 43:10308–10313.
23. Zhu, Y., J. E. Graham, …, D. A. Bryant. 2010. Roles of xanthophyll carotenoids in protection against photoinhibition and oxidative stress in the cyanobacterium *Synechococcus* sp. strain PCC 7002. *Arch. Biochem. Biophys.* 504:86–99.
24. Aro, E. M., I. Virgin, and B. Andersson. 1993. Photoinhibition of Photosystem II. Inactivation, protein damage and turnover. *Biochim. Biophys. Acta.* 1143:113–134.
25. Vass, I. 2011. Role of charge recombination processes in photodamage and photoprotection of the photosystem II complex. *Physiol. Plant.* 142:6–16.
26. Finazzi, G., G. N. Johnson, …, F. A. Wollman. 2006. Nonphotochemical quenching of chlorophyll fluorescence in *Chlamydomonas reinhardtii*. *Biochemistry.* 45:1490–1498.
27. Ruban, A. V., J. Lavaud, …, A. L. Etienne. 2004. The super-excess energy dissipation in diatom algae: comparative analysis with higher plants. *Photosynth. Res.* 82:165–175.
28. Ruban, A. V., R. Berera, …, R. van Grondelle. 2007. Identification of a mechanism of photoprotective energy dissipation in higher plants. *Nature.* 450:575–578.
29. Holt, N. E., D. Zigmantas, …, G. R. Fleming. 2005. Carotenoid cation formation and the regulation of photosynthetic light harvesting. *Science.* 307:433–436.
30. Wilson, A., G. Ajlani, …, D. Kirilovsky. 2006. A soluble carotenoid protein involved in phycobilisome-related energy dissipation in cyanobacteria. *Plant Cell.* 18:992–1007.
31. Kerfeld, C. A., M. R. Sawaya, …, T. O. Yeates. 2003. The crystal structure of a cyanobacterial water-soluble carotenoid binding protein. *Structure.* 11:55–65.
32. Wilson, A., J. N. Kinney, …, C. A. Kerfeld. 2010. Structural determinants underlying photoprotection in the photoactive orange carotenoid protein of cyanobacteria. *J. Biol. Chem.* 285:18364–18375.
33. Gwizdala, M., A. Wilson, and D. Kirilovsky. 2011. In vitro reconstitution of the cyanobacterial photoprotective mechanism mediated by the orange carotenoid protein in *Synechocystis* PCC 6803. *Plant Cell.* 23:2631–2643.
34. Gorbunov, M. Y., F. I. Kuzminov, …, P. G. Falkowski. 2011. A kinetic model of non-photochemical quenching in cyanobacteria. *Biochim. Biophys. Acta.* 1807:1591–1599.
35. Rakhimberdieva, M. G., I. V. Elanskaya, …, N. V. Karapetyan. 2010. Carotenoid-triggered energy dissipation in phycobilisomes of *Synechocystis* sp. PCC 6803 diverts excitation away from reaction centers of both photosystems. *Biochim. Biophys. Acta.* 1797:241–249.
36. Ajlani, G., and C. Vernotte. 1998. Construction and characterization of a phycobiliprotein-less mutant of *Synechocystis* sp. PCC 6803. *Plant Mol. Biol.* 37:577–580.
37. Ughy, B., and G. Ajlani. 2004. Phycobilisome rod mutants in *Synechocystis* sp. strain PCC6803. *Microbiology.* 150:4147–4156.
38. Stokkum, I. H. M., B. Oort, …, H. Amerongen. 2008. (Sub)-Picosecond spectral evolution of fluorescence studied with a synchroscan streak-camera system and target analysis. *In* Biophysical Techniques in Photosynthesis. T. J. Aartsma and J. Matysik, editors. Springer, Amsterdam, The Netherlands. 223–240.
39. van Oort, B., A. Amunts, …, R. Croce. 2008. Picosecond fluorescence of intact and dissolved PSI-LHCI crystals. *Biophys. J.* 95:5851–5861.

40. Van Oort, B., S. Murali, …, H. van Amerongen. 2009. Ultrafast resonance energy transfer from a site-specifically attached fluorescent chromophore reveals the folding of the N-terminal domain of CP29. *Chem. Phys.* 357:113–119.

41. Laptenok, S. P., J. W. Borst, …, H. van Amerongen. 2010. Global analysis of Förster resonance energy transfer in live cells measured by fluorescence lifetime imaging microscopy exploiting the rise time of acceptor fluorescence. *Phys. Chem. Chem. Phys.* 12:7593–7602.

42. Mullen, K. M., and I. H. M. van Stokkum. 2007. TIMP: An R package for modeling multi-way spectroscopic measurements. *J. Stat. Softw.* 18:1–46.

43. Snellenburg, J. J., S. P. Laptenok, …, I. H. M. Van Stokkum. 2011. Glotaran: a Java-based graphical user interface for the R-package TIMP. *J. Stat. Softw.* In press.

44. van Stokkum, I. H. M., D. S. Larsen, and R. van Grondelle. 2004. Global and target analysis of time-resolved spectra. *Biochim. Biophys. Acta.* 1657:82–104.

45. Rakhimberdieva, M. G., F. I. Kuzminov, …, N. V. Karapetyan. 2011. *Synechocystis* sp. PCC 6803 mutant lacking both photosystems exhibits strong carotenoid-induced quenching of phycobilisome fluorescence. *FEBS Lett.* 585:585–589.

46. van Stokkum, I. H. M., B. Gobets, …, J. T. Kennis. 2006. (Sub)-picosecond spectral evolution of fluorescence in photoactive proteins studied with a synchroscan streak camera system. *Photochem. Photobiol.* 82:380–388.

47. Wilson, A., C. Punginelli, …, D. Kirilovsky. 2008. A photoactive carotenoid protein acting as light intensity sensor. *Proc. Natl. Acad. Sci. USA.* 105:12075–12080.